

Heat transfer performance of slush nitrogen in a horizontal circular pipe

Yijian Li^{a,b}, Tao Jin^{a,*}, Shuqin Wu^a, Jianjian Wei^a, Jun Xia^b, Tassos G. Karayiannis^b

^a Institute of Refrigeration and Cryogenics/Key Laboratory of Refrigeration and Cryogenic Technology of Zhejiang Province, Zhejiang University, Hangzhou 310027, China

^b Department of Mechanical and Aerospace Engineering & Institute of Energy Futures, Brunel University London, Uxbridge UB8 3PH, UK

ARTICLE INFO

Keywords:

Slush nitrogen
HTS
Cryogenic multiphase flow
Forced convection
Heat transfer deterioration

ABSTRACT

Slush nitrogen is considered to be a potential coolant for high temperature superconducting cables. In this study, the heat transfer characteristics of slush nitrogen flow in a horizontal circular pipe were experimentally and numerically studied. The numerical results for the heat transfer coefficient agree well with the experimental results, with the relative errors within $\pm 10\%$. The effect of the particle concentration and size, the pipe size and the flow velocity on the forced convection of slush nitrogen and the solid-liquid interfacial heat transfer were discussed. The heat transfer coefficient in the slush nitrogen pipe flow is found to be lower than that of the subcooled liquid nitrogen (at 63.15 K) at the same flow velocity and to decrease with increasing solid fraction. The mechanism of the heat transfer deterioration phenomenon of slush nitrogen was analyzed. In addition, a modified experimental empirical correlation for the Nusselt number of slush nitrogen flow was obtained, which can be applicable for different flow regimes (i.e., homogenous flow, heterogeneous flow and sliding bed flow). The correlation considered the influence of particle conditions on the interfacial heat and mass transfer and has an accuracy within $\pm 10\%$.

1. Introduction

The power loss due to the resistance of transmission lines is considerable, which can be approximately 7%–8% of the total electricity generation in China. The application of high temperature superconducting (HTS) cables has drawn much attention since the discovery of high temperature superconducting materials by Bednorz and Muller in 1986 [1]. With the help of the HTS cables with no electrical resistance, the maximum current capacity could be considerably larger than that of the traditional transmission line. The HTS cables with a critical temperature higher than 77 K can be cooled by forced flow of subcooled liquid nitrogen [2]. One issue for the adoption of liquid nitrogen is that the local instant high heat flux of the HTS cables could induce the vaporization of liquid nitrogen and even a localized thermal shock, which could further lead to integral quenched disorder of the superconductors. In 2004, Ishimoto et al. [3] proposed that slush nitrogen, a low temperature two-phase fluid with solid particles suspended in the liquid, could be a new type of coolant for HTS cables. Superior to the subcooled liquid nitrogen, the slurry has lower temperature, higher heat capacity and density, which can help to reduce the risk of superconductor quenching, reduce the size of the cooling system and contribute to lower storage and transport costs.

The heat transfer performance of slush nitrogen is one of the main

concerns for its application in HTS cables. In 2003, Ohira [4] conducted experimental investigations on the nucleate boiling heat transfer of slush hydrogen or slush nitrogen, and found that the critical heat flux values of slush hydrogen and slush nitrogen decrease to 0.45 and 0.62 times those of the liquids at the normal-boiling-point temperature in the case of horizontal facing-up surface. Recently, the experimental and numerical researches on the heat transfer of slush nitrogen were mainly focused on the flow in horizontal pipes, considering its potential application in the cooling of HTS cables. Matsuo et al. [5] conducted an experimental investigation on the heat transfer characteristics of slush nitrogen in a horizontal pipe and found that the Nusselt number of slush nitrogen was higher than that of ordinary single-phase fluid flow with a low Reynolds number and then gradually approached the Nusselt number of the single-phase fluid as the Reynolds number was increased. Zhang and Jiang [6] also found that the heat transfer coefficient of slush nitrogen was higher than that of subcooled liquid nitrogen under the same conditions and increased with increasing solid fraction. On the other hand, Ohira et al. [7,8] carried out experiments to study the local heat transfer coefficient of slush nitrogen flow in pipes with various sizes and shapes, and the heat transfer deterioration phenomenon (i.e., the heat transfer coefficient for slurry flow can be lower than that of the subcooled liquid) occurred for slush nitrogen when the flow velocity was high enough, e.g., at a flow velocity over 2.0 m/s in the pipe with

* Corresponding author.

E-mail address: jintao@zju.edu.cn (T. Jin).

<https://doi.org/10.1016/j.tsep.2018.08.001>

Received 7 December 2017; Received in revised form 19 June 2018; Accepted 1 August 2018

2451-9049/© 2018 Elsevier Ltd. All rights reserved.

Nomenclature

C_D	drag coefficient, –
C_L	lift coefficient, –
C_{VM}	virtual mass coefficient, –
D	pipe diameter, m
d_s	particle diameter, m
e_{ss}	restitution coefficient for particles, –
e_{sw}	restitution coefficient for particles and wall, –
$\vec{F}_{D,q}$	drag force, N
$\vec{F}_{L,q}$	lift force, N
$\vec{F}_{VM,q}$	virtual mass force, N
Fr	Froude number, –
G_k	generation of turbulence kinetic energy, $\text{kg}/(\text{m}^3\text{s}^3)$
\vec{g}	gravitational acceleration, m^2/s
$g_{0,ss}$	radial distribution function, –
$g(V')$	breakage frequency, –
h	enthalpy, kJ/kg
h_{pq}	interphase heat transfer coefficient, $\text{kJ}/(\text{kg}\cdot\text{K})$
h_{melt}	melting latent heat, kJ/kg
k	turbulence kinetic energy, m^2/s^2
k_{Θ_s}	diffusion coefficient, –
L	pipe length, m
\dot{m}	mass flow, kg/s
\dot{m}_{pq}	interphase mass transfer, kg/s
Nu	Nusselt number, –
$n(V', t)$	number density function, –
Pr	Prandtl number, –
p	pressure, Pa
p_s	solids pressure, Pa
\vec{q}	heat flux, W/m^2

Re	Reynolds number, –
Re_p	particle Reynolds number, –
Ste	Stefan number, –
T	temperature, K
t	time, s
\vec{U}_{sw}	particle slip velocity parallel to the wall, m/s
V	daughter particle volume, m^3

Greek Letters

α	volume fraction, %
$\alpha_{s,max}$	the packing limit, %
β	effective viscosity parameter, –
$\beta(V V')$	breakage probability density function, –
δ	measurement uncertainty, –
ε	rate of dissipation, m^2/s^3
ϕ	specularity coefficient, –
ϕ_{ls}	interphase energy exchange, $\text{kg}/(\text{m}^3\text{s}^3)$
γ_{Θ_s}	collisional dissipation of energy, $\text{kg}/(\text{m}^3\text{s})$
$[\eta]$	intrinsic viscosity, $\text{Pa}\cdot\text{s}$
μ	fluid viscosity, $\text{Pa}\cdot\text{s}$
μ_{lw}	fluid viscosity near wall, $\text{Pa}\cdot\text{s}$
Π_k, Π_ε	turbulent interaction source term, –
Θ_s	granular temperature, m^2/s^2
ρ	density, kg/m^3
$\bar{\tau}$	shear stress, Pa

Subscripts

l	liquid phase
s	solid phase
sl, m	slush
w	wall
p	either solid phase or liquid phase
q	the opposite phase of p

an inner diameter of 10 mm.

Studies on the heat transfer of ambient slurry flow also have discussed about the heat transfer deterioration phenomenon of ambient slurry flow. Knodel et al. [9] experimentally studied the heat transfer of ice slurries in a horizontal tube and found that the heat transfer coefficient of ice slurry was lower than that of water and decreased with increasing ice fraction. Liu et al. [10] reported that for the HDPE-water suspension with a particle size of 3.2 mm, the heat transfer performance in the horizontal pipe increased with increasing particle concentration, while for the suspension with a particle size of 1.3 mm, the heat transfer performance deteriorated comparing to that of pure water. The heat transfer characteristics of the slurry flow in the horizontal pipes depend on the flow pipe configuration, flow velocity, and solid fraction. At present, how the particle motion affects the forced convection heat transfer has not yet been well understood.

Computational Fluid Dynamics (CFD) has also been adopted for the prediction of flow and heat transfer characteristics of slush nitrogen. Ishimoto et al. [11] built a transient numerical model based on the Euler-Lagrange single-fluid approach to simulate the slush nitrogen flow in a horizontal circular pipe and a converging-diverging pipe, which is applicable for very dilute particulate flow. The simulations presented that at the high Reynolds number, the pressure drop of slush nitrogen slurry was lower than that of the liquid nitrogen under the same conditions. Ohira et al. [12] constructed a 3-D numerical model to investigate the flow and heat transfer characteristics of cryogenic slush fluids in a horizontal circular pipe, where the particle collisions were neglected and the heat transfer deterioration phenomenon that was found in the experiments was not considered. So far, the modeling of solid particles in previous two-fluid models was based on the hypothesis of a constant diameter, which neglected the influence of the particle size distribution on interfacial momentum and energy transfer. Jin et al.

[13,14] built a two-fluid numerical model coupled with population balance equations for slush nitrogen flow, in which the particle size distribution was calculated by the population balance equations to account for the influence of particle size on interfacial interactions. The heat transfer deterioration phenomenon was confirmed in the numerical analysis [13].

The experimental data for flow and heat transfer of slush nitrogen are not yet sufficient and comprehensive. Ohira et al. [7] claimed that the heat transfer coefficient of slush nitrogen in horizontal pipes was lower than that of subcooled liquid nitrogen while Matsuo et al. [5] and Jiang et al. [6] claimed the heat transfer coefficient increases with increasing solid fraction, thus the results about the heat transfer deterioration phenomenon of slush nitrogen from different researches are even in discrepancy. Hence, the experimental empirical correlations and numerical models still need further verification. In particular, the heat transfer deterioration phenomenon of slush nitrogen requires further proof and related theoretical discussion. In this study, an experimental apparatus for the flow and heat transfer test of slush nitrogen in a horizontal circular pipe with a diameter of 16 mm was constructed. The heat transfer coefficients were obtained for slush nitrogen flow with an inlet velocity of 0–4 m/s, a solid volume fraction of 0–23% and a wall heat flux of 12–15 kW/m^2 . An experimental empirical correlation for the Nusselt number with the slush Reynolds number of slush nitrogen flow is then proposed. The Euler-Euler two-fluid model coupled with the population balance equations [13] is constructed for slush nitrogen flow. Based on the experimental and numerical results, the heat transfer deterioration of slush nitrogen in a horizontal pipe with various particle concentration and size, pipe size and flow velocity is discussed.

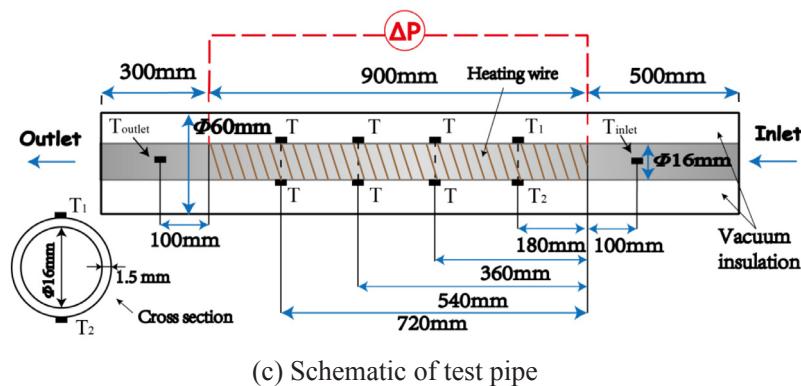
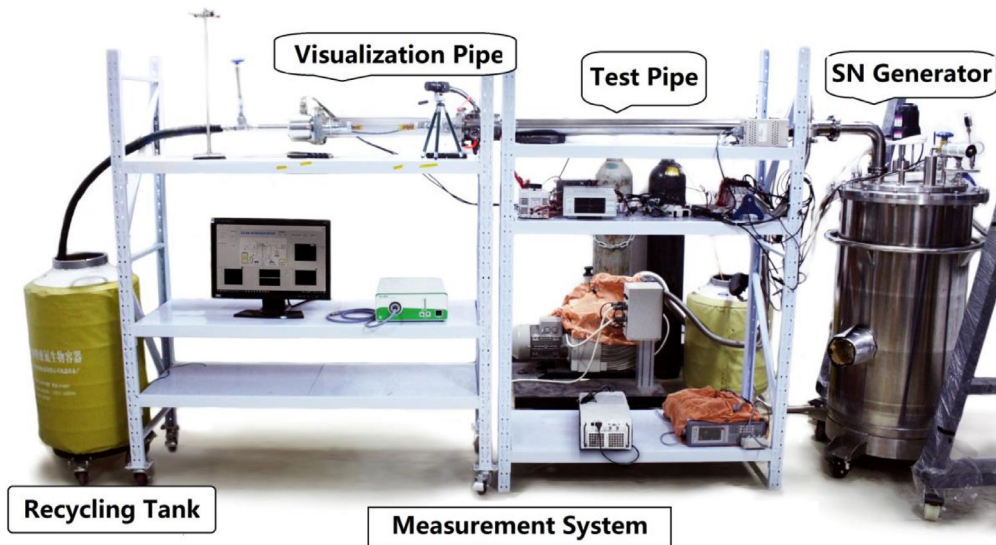
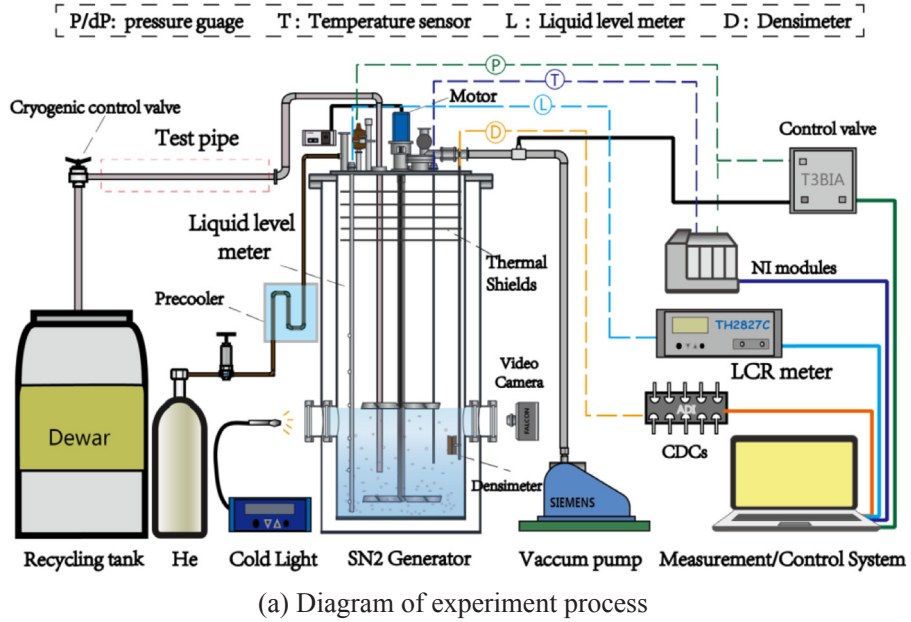


Fig.1. Experimental apparatus for the flow and heat transfer test of slush nitrogen.

2. Experimental and numerical methodology

2.1. Experimental apparatus and measurement methods

The experimental setup for the flow and heat transfer tests of slush nitrogen in a horizontal pipe is given in Fig. 1, which mainly consists of the slush nitrogen production system, the flow and heat transfer test pipe and the measurement/control system. The preparation tank with a capacity of 80 L was used for the production of slush nitrogen. Two sets of four-blade impellers were installed at two positions (upper and lower) inside the tank to break the solid nitrogen layer and to enhance the liquid convection, so as to improve the crashing effect of the particles.

The freeze-thaw method was adopted for the production of slush nitrogen with the freeze-thaw cycle of 15 s - 15 s and a pumping rate of 9 L/s. The average diameter of solid nitrogen particles was about 1.5 mm, which was obtained by image analysis based on high-speed photography. The solid fraction of slush nitrogen was measured by a capacitance-type densimeter, whose electrodes are composed of a square plate and two symmetrically positioned cylinders. The densimeter has high linearity and accuracy, with a measurement error

of ± 0.16%. The liquid level of slush nitrogen was measured by a capacitance-type liquid level meter, which is equipped with a three-layer coaxial tube, where the inner two layers are capacitor electrodes and the outermost one is shielding layer. The measurement error of the liquid level meter is ± 1%. The liquid level meter was also used to measure the flow velocity of slush nitrogen in the flow test pipe. More details about the capacitance-type densimeter and liquid level meter can be found in our earlier work [15].

Precooled helium gas was used to pressurize the tank to 0.1–0.3 MPa, and thus to transfer slush nitrogen into the horizontal flow pipe, where the flow and heat transfer tests are carried out. The flow rate was controlled by a cryogenic control valve equipped at the end of the flow pipe, and calculated by the liquid level change in the tank, which was measured by the capacitance-type liquid level meter. The horizontal flow test pipe consists of three segments, among which the length of the upstream segment was 500 mm to ensure the full development of the flow. The downstream segment of 300 mm was used to reduce the heat leakage at the end of the flow pipe, and the test segment was a 900 mm-long Grade-304 stainless steel pipe with an inner diameter of 16 mm and an outside diameter of 19 mm. A differential pressure transmitter was used to measure the pressure drop of the

Table 1
Mathematical equations for the present modeling.

Conservation equations

$$\frac{\partial}{\partial t}(\alpha_q \rho_q) + \nabla \cdot (\alpha_q \rho_q \vec{v}_q) = \dot{m}_{pq} - \dot{m}_{qp} \tag{3}$$

$$\frac{\partial}{\partial t}(\alpha_q \rho_q \vec{v}_q) + \nabla \cdot (\alpha_q \rho_q \vec{v}_q \vec{v}_q) = -\alpha_q \nabla p + \nabla \cdot \vec{\tau}_q + \alpha_q \rho_q \vec{g} + \vec{R}_{pq} + (\dot{m}_{pq} \vec{v}_p - \dot{m}_{qp} \vec{v}_q) \tag{4}$$

$$\nabla \cdot (\alpha_q \rho_q h_q) - \nabla \cdot (\alpha_q \rho_q \vec{v}_q h_q) = \vec{\tau}_q \cdot \nabla \vec{v}_q - \nabla \cdot \vec{q}_q + h_{pq}(T_p - T_q) + \dot{m}_{pq} h_{melt} \tag{5}$$

Interphase momentum exchange

$$\vec{F}_{L,q} = -C_L \alpha_s \rho_l (\vec{v}_l - \vec{v}_s) \times (\nabla \times \vec{v}_l) \tag{6}$$

$$C_L = \frac{3}{2\pi \sqrt{Re_w}} C_L' \quad C_L' = 6.46 \tag{7}$$

$$\vec{F}_{VM} = C_{VM} \alpha_s \rho_l \left(\frac{d\vec{v}_l}{dt} - \frac{d\vec{v}_s}{dt} \right) \quad C_{VM} = 0.5 \tag{8}$$

$$\vec{F}_D = K_{sl} |\vec{v}_l - \vec{v}_s| \tag{9}$$

$$C_D = \max \left[\frac{24}{Re_p} (1 + 0.15 Re_p^{0.687}), 0.44 \right] \tag{10}$$

$$Re_p = \rho_l d_s |\vec{v}_s - \vec{v}_l| / \mu_m \tag{11}$$

$$\mu_m = \mu_l \exp \left\{ \frac{2.5}{\beta} \left[\frac{1}{(1 - \alpha_s)^\beta} - 1 \right] \right\} \tag{12}$$

Interphase heat and mass transfer

$$h_{pq} = 6 \lambda_l \alpha_s Nu_{sl} / d_s^2 \tag{13}$$

$$\dot{m}_{pq} = h_{pq} (T_p - T_q) / h_{melt} \tag{14}$$

$$Nu_{sl} = (7 - 10\alpha_l + 5\alpha_l^2)(1 + 0.7 Re_p^{0.2} Pr^{1/3}) + (1.33 - 2.4\alpha_l + 1.2\alpha_l^2) Re_p^{0.7} Pr^{1/3} \tag{15}$$

Granular temperature equations

$$\frac{3}{2} \left[\frac{\partial}{\partial t} (\alpha_s \rho_s \Theta_s) + \nabla \cdot (\alpha_s \rho_s \vec{v}_s \Theta_s) \right] = (-p_s \vec{I} + \vec{\tau}_s) \cdot \nabla \vec{v}_s + \nabla \cdot (k_{\Theta_s} \nabla \Theta_s) - \gamma_{\Theta_s} + \phi_{ls} \tag{16}$$

$$\vec{\tau}_s = -\frac{\pi}{6} \sqrt{3} \phi \frac{\alpha_s}{\alpha_{s,max}} \rho_s g_{0,ss} \Theta_s^{1/2} \vec{U}_{sw} \tag{17}$$

$$q_s = \frac{\pi}{6} \sqrt{3} \phi \frac{\alpha_s}{\alpha_{s,max}} \rho_s g_{0,ss} \Theta_s^{1/2} \vec{U}_{sw} - \frac{\pi}{4} \sqrt{3} \frac{\alpha_s}{\alpha_{s,max}} (1 - e_{sw}^2) \rho_s g_{0,ss} \Theta_s^{3/2} \tag{18}$$

Population balance equations

$$\frac{\partial}{\partial t} [n(V, t)] + \nabla \cdot [\vec{u} n(V, t)] + \nabla_V \cdot \left[\frac{\partial V}{\partial t} n(V, t) \right] = \int_{\Omega_V} pg(V') \beta(V|V') n(V', t) dV' - g(V) n(V, t) \tag{19}$$

$$g(V') = K_b \vec{v}^2 L^{5/3} \tag{20}$$

$$\beta(V|V') = 0.5 \left[\frac{C}{V'} + \frac{1-C/2}{V'} \left\{ 24 \left(\frac{V}{V'} \right)^2 - 24 \left(\frac{V}{V'} \right) + 6 \right\} \right] \tag{21}$$

$$m_k = \int_0^\infty L^k n(L) dL \approx \sum_{i=1}^N L_i^k w_i \quad k = 0, 1, \dots, N-1 \tag{22}$$

$$d_{32} = \frac{\sum N_k L_k^3}{\sum N_k L_k^2} \tag{23}$$

Standard k-ε model

$$\frac{\partial(\alpha_l \rho_l k)}{\partial t} + \nabla \cdot (\alpha_l \rho_l \vec{v}_l k) = \nabla \cdot \left[\left(\mu_l + \frac{\mu_{t,l}}{\sigma_k} \right) \nabla k \right] + G_k - \alpha_l \rho_l \epsilon + \Pi_k \tag{24}$$

$$\frac{\partial(\alpha_l \rho_l \epsilon)}{\partial t} + \nabla \cdot (\alpha_l \rho_l \vec{v}_l \epsilon) = \nabla \cdot \left[\left(\mu_l + \frac{\mu_{t,l}}{\sigma_\epsilon} \right) \nabla \epsilon \right] + C_{1\epsilon} \frac{\epsilon}{k} G_k - C_{2\epsilon} \alpha_l \rho_l \frac{\epsilon^2}{k} + \Pi_\epsilon \tag{25}$$

slush nitrogen flow, with a measuring range of 0–35 kPa and an accuracy of $\pm 0.5\%$. The test pipe was uniformly wound with Manganese copper heating wire and the heat flux was controlled within the range of 12–15 kW/m². Two platinum resistance thermometers (with an accuracy of ± 0.1 K at the temperature ranging from 50 to 300 K) were inserted into the inlet and the outlet of test section to measure the fluid temperature, and the mounting holes were sealed with cryogenic epoxy glue. T-type thermocouples (with an accuracy of ± 0.1 K at the temperatures ranging from 50 to 300 K) were located every 180 mm along test pipe. The temperatures at the top and the bottom of the pipe were measured to obtain the average wall temperature. The test pipe was wrapped with multi-layer thermal radiation insulation materials and an outer pipe with a diameter of 66 mm was equipped for interlayer vacuum insulation to minimize the thermal leakage and the vacuum degree inside the interlayer is 10^{-3} Pa. The overall heat leakage of the flow test pipe, including the radiation heat leakage and the axial heat conduction from the pipe ends, was estimated to be 2.51 W for a heating power of 650 W. The measurement errors for pipe length and diameter were ± 0.1 mm. The measurement uncertainty for wall heat flux can be obtained by

$$\delta_q = \sqrt{\delta_Q^2 + \delta_D^2 + \delta_L^2} \quad (1)$$

where δ_Q is the measurement uncertainty of heat power, $\delta_Q = \pm 0.39\%$. δ_D is the measurement uncertainty of pipe diameter, $\delta_D = \pm 0.53\%$. δ_L is the measurement uncertainty of pipe length, $\delta_L = \pm 0.01\%$. Thus, the measurement uncertainties for wall heat flux were $\pm 0.66\%$. The measurement uncertainty for local heat transfer coefficient can be obtained by

$$\delta_h = \sqrt{\delta_q^2 + \delta_T^2} \quad (2)$$

where δ_T is the measurement uncertainty of temperature. For the temperature difference of 5 K, $\delta_T = \pm 2\%$. Thus, the measurement uncertainty for local heat transfer coefficient was $\pm 2.11\%$.

2.2. Numerical modeling

An Euler-Euler two-fluid model based on population balance equations was built to predict the flow and heat transfer characteristics of slush nitrogen in a horizontal pipe [13]. The equations for the numerical model are given in Table 1, where the subscripts q represents either s (solid phase) or l (liquid phase), and p is the second phase l or s , accordingly.

For the Euler-Euler two-fluid model, the solid and liquid phases of slush nitrogen are mathematically treated as interpenetrating continua. The mass, momentum and energy conservation equations for each phase are given as Eqs. (3–5), where \dot{m}_{pq} is the interphase mass exchange, $(\dot{m}_{pq}\vec{v}_p - \dot{m}_{qp}\vec{v}_q)$ is the momentum transfer arising from the interphase mass exchange, and \vec{R}_{pq} is the interphase momentum exchange. \vec{R}_{pq} consists of lift force, virtual mass force and drag force, given by Eqs. (6–10). To calculate the drag force, the slush effective viscosity μ_m is used, instead of liquid viscosity, as given by Eq. (12), which is derived by Cheng and Law [16]. β is the sole empirical parameter to account for the shape, size and type of solid particle, ranging from 0.95 to 3.9, which can take the value of 1.5 for slush nitrogen [14]. The slush effective viscosity is also adopted to calculate the interphase heat and mass transfer, as Eqs. (13–15). The modifications of the drag law and the interphase mass transfer coefficients with the slush effective viscosity help to consider the influence of solid viscosity on the interfacial heat and mass transfer.

The momentum equation of the solid phase is closed by the granular temperature equation, as given by Eqs. (16–18). Θ_s is the granular temperature, defined by $\Theta_s = 1/3u_{s,i}u_{s,i}$, representing the kinetic energy of the particles' random motion, and $u_{s,i}$ is the fluctuating solid velocity. ϕ is the specularly coefficient between the particle and the wall, whose

value ranges from 0 to 1 depending on the surface conditions of both the wall and the particles and is set to 0.01 for slush nitrogen [14].

To take into account the influence of particle size on the interfacial heat and mass transfer, the population balance equations, as given by Eq. (19), are used to analyze the evolution of particle size distribution [17]. On the right side of Eq. (19), the two terms are the birth and death terms due to breakage, respectively. $g(V')\beta(V|V')$ is the breakage rate, where $g(V')$ is the breakage frequency and $\beta(V|V')$ is the probability density function of particles breaking from volume V' to volume V . The breakage kernels can be calculated by Eq. (20), and the probability density function is solved by the parabolic form as Eq. (21). The population balance equations is solved by the Quadrature Method of Moments (QMOM), which is based on the quadrature approximation with the internal coordinates of particle length [18,19]. By using the QMOM approach, only the lower order moments of the transport equations need to be solved.

In the present CFD analysis, the standard $k-\varepsilon$ model is used for predicting the turbulent quantities. The turbulence kinetic energy k and its rate of dissipation ε are obtained by Eqs. (24 and 25), respectively. The model constants are set to $C_{1\varepsilon} = 1.44$, $C_{2\varepsilon} = 1.92$, $C_\mu = 0.09$, $\sigma_k = 1.0$, and $\sigma_\varepsilon = 1.3$ [20]. Referring to the physical model of test pipe, a horizontal circular pipe with the length of 1000 mm and the inner diameter of 16 mm is employed in the simulation, as shown in Fig. 2. The X coordinate is the flow direction, the Y coordinate is the vertical direction, and the gravity direction is -Y coordinate, with a gravity acceleration of $g = 9.8$ m/s². The grid-independence analysis results for the particle concentration is given in Fig. 3, thus the structured computational grids with a cell quantity of 380,000 have been adopted for the numerical simulation. The grids are refined at the wall boundary layer with the minimum width near the pipe wall of 0.13 mm, and the grid in the flow direction is even. The standard $k-\varepsilon$ model is used for predicting the turbulent quantities. The dimensionless wall distance y^+ for the cell adjacent to the wall $y = +0.03 \sim 1.2$, which fulfills the requirement of the enhanced wall function.

3. Results and discussions

3.1. Heat transfer of subcooled liquid nitrogen

Fig. 4 presents the experimental and CFD results for heat transfer coefficient of subcooled liquid nitrogen (at 63.15 K), compared with the empirical equations. The theoretical Nusselt number is calculated by Seider-Tate equation for turbulent flow [21]

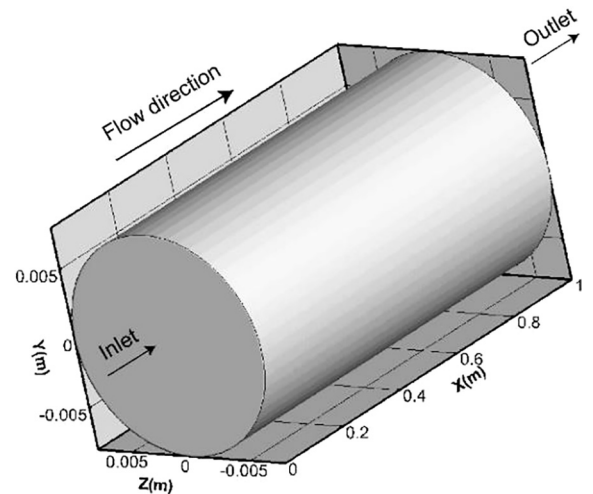


Fig. 2. Numerical domain for slush nitrogen flow.

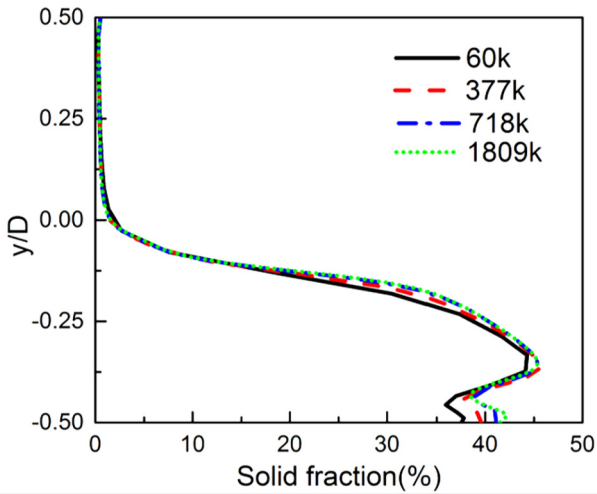


Fig. 3. Grid-independence analysis results for particle concentration.

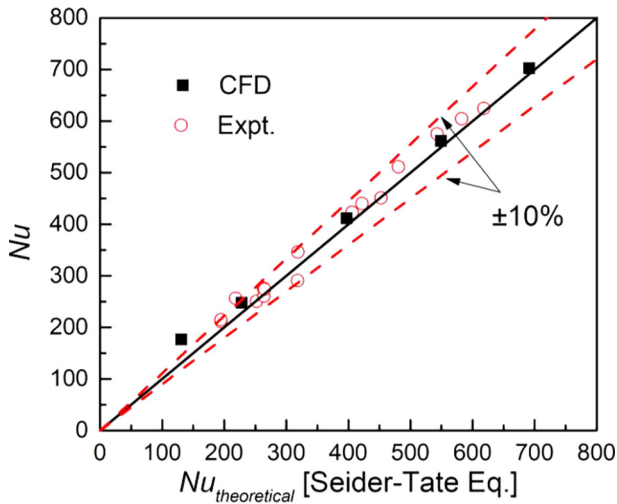


Fig. 4. Results for the Nusselt number of subcooled liquid nitrogen.

$$Nu = 0.027Re^{0.8}Pr^{1/3} \left(\frac{\mu_l}{\mu_{hw}} \right)^{0.14} \quad (26)$$

where μ_l is the bulk viscosity, μ_{hw} is the viscosity evaluated at the wall temperature. The Reynolds number and Prandtl number are defined by the physical properties of the bulk fluid.

The local heat transfer coefficient is calculated by

$$h_{local} = \vec{q} / (T_w - T_f) \quad (27)$$

where \vec{q} is the heat flux, which is approximately 12 kW/m². T_f is the local bulk temperature and T_w is the temperature of the inner wall. Since the local temperature of the inner wall is difficult to measure in the experiments, the temperature of the outer wall is measured and the temperature of the inner wall was calculated by

$$T_w = T_{w,o} - \frac{\vec{q}d}{2\lambda_{wall}} \ln(D/d) \quad (28)$$

where $T_{w,o}$ is the temperature of the outer wall, measured by thermocouples. λ_{wall} is the thermal conductivity of stainless steel, which is obtained from the average value of thermal conductivities in the temperature range of 63–80 K, i.e., 7.5 W/m·K. D and d are the outer and inner diameters of test pipe, respectively. The temperature of the bulk fluid in the experiments is predicted by

$$T_f = T_{in} + \frac{X}{L} (T_{out} - T_{in}) \quad (29)$$

where T_{in} is the temperature at the inlet of test pipe, and T_{out} is the temperature at the outlet of test pipe. X is the distance from the temperature measuring point to the inlet. The heat transfer coefficient decreases along the pipe in the entrance region and becomes steady in the fully developed region [11]. Hence, all of the local heat transfer coefficients given below are measured at $x = 720$ mm, where the slurry flow is fully developed. The length of test pipe is $L = 900$ mm.

As shown in Fig. 4, both experimental and numerical results for the Nusselt number agree well with that of Eq. (26), with the deviations within $\pm 10\%$, indicating that the experimental system is effective for measuring pressure drop and heat transfer coefficient. In addition, the CFD results show good agreements with the experimental results and empirical equations.

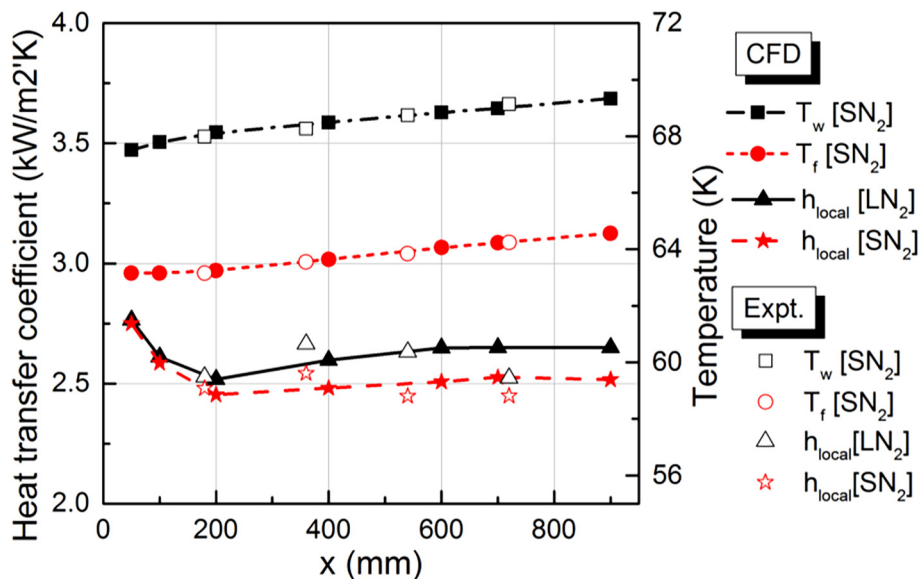


Fig. 5. Results for temperature and heat transfer coefficient along the flow pipe.

3.2. Heat transfer coefficients of slush nitrogen

Fig. 5 shows the experimental and numerical results for the wall temperature T_w , bulk fluid temperature T_f and local heat transfer coefficient h_{local} distribution along the pipe. The numerical results are for the subcooled liquid nitrogen and slush nitrogen ($\alpha_s = 10\%$) at a velocity of 1.0 m/s, while the experimental results are for the subcooled liquid nitrogen and slush nitrogen ($\alpha_s = 11.1\%$) at a velocity of 1.09 m/s. It can be seen that the numerical simulation results of the heat transfer coefficient are in good agreement with the experimental results for both the temperature and heat transfer coefficient distributions. The heat transfer coefficients for liquid nitrogen are slightly higher than that of slush nitrogen, which indicates that the heat transfer performance of the slush nitrogen in the horizontal circular pipe is worse than that of the liquid nitrogen at the triple point.

As the flow develops in the pipe, the fluid temperature and the wall temperature both gradually rise. The heat transfer coefficients at the inlet decrease with flow development and become constant when $x > 300$ mm. Fig. 6 presents the solid velocity profiles and the liquid phase temperature distributions of slush nitrogen ($\alpha_s = 10\%$) along the test pipe with an initial flow velocity of 1.0 m/s. The velocity and temperature profiles both show greater gradients when the flow is in the developing region. When the flow fully developed, the velocity profiles are almost constant and the temperature rises with a constant rate, indicating constant laminar and thermal boundary layers in the fully developed region. It can be concluded that the heat transfer coefficient decreases in the inlet region because the thickness of laminar layer increases with flow development. When fully developed, the thickness of laminar layer is constant and the heat transfer coefficient is almost constant.

Fig. 7 presents the experimental and CFD results for the local heat transfer coefficient of slush nitrogen, where the slush nitrogen flow in a pipe with the wall heat flux of 12–15 kW/m² is experimentally and numerically studied with the inlet flow velocity of 0–4 m/s and the inlet solid fraction of 0–23%. The experimental and CFD results show good agreement with a relative error within $\pm 10\%$. Generally, the heat transfer coefficient of slush nitrogen increases with increasing flow velocity and decreases with the increasing solid fraction, which indicates that the heat transfer performance of slush nitrogen flow deteriorates with increasing concentration of solid particles. It is noted that the heat transfer performance of slush nitrogen is worse than that of liquid nitrogen and the gap becomes wider when the velocity is increased.

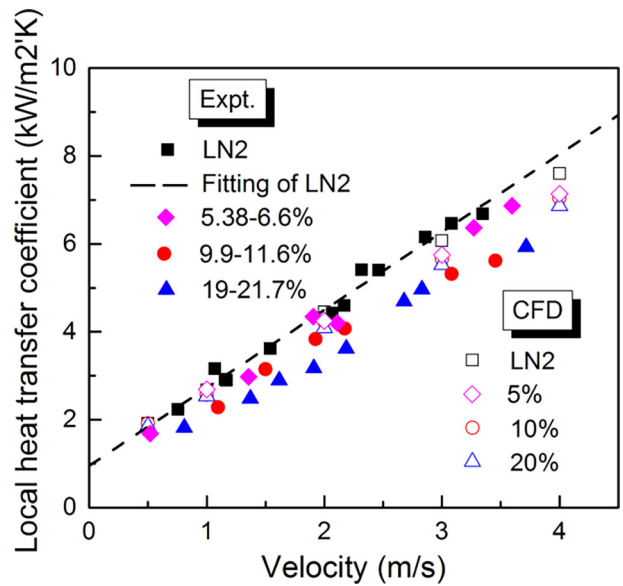


Fig. 7. Results for local heat transfer coefficient of slush nitrogen.

3.3. Heat transfer deterioration of slush nitrogen

The effect of the particle concentration and size, the pipe size and the flow velocity on the forced convection of slush nitrogen and the solid-liquid interfacial heat transfer have been analyzed to better understand the mechanism for the heat transfer deterioration of slush nitrogen compared that of subcooled liquid nitrogen. Fig. 8 shows the temperature distribution at $x = 720$ mm for the subcooled liquid nitrogen and the slush nitrogen ($\alpha_s = 10\%$) with an inlet flow velocity of 0.5 m/s. It can be seen that the temperature distribution of the subcooled liquid nitrogen is symmetric along the centerline, while the temperature is relatively low in the lower half of the pipeline for slush nitrogen, due to particle deposition. Fig. 9 gives the contours of the particle concentration distribution at $x = 720$ mm with the inlet solid fractions of 10% and 20%, respectively, and an inlet velocity of 0.5 m/s. For the slush nitrogen flow with higher particle concentration, the particles concentrate denser in the lower part of the pipe. Moreover, the particle fraction near the upper part is less than 2%.

Fig. 10 gives the temperature variations of the wall and the slush nitrogen with solid volumetric fraction at velocity of 0.5 m/s and location of $x = 720$ mm. The bulk fluid temperature of slush nitrogen

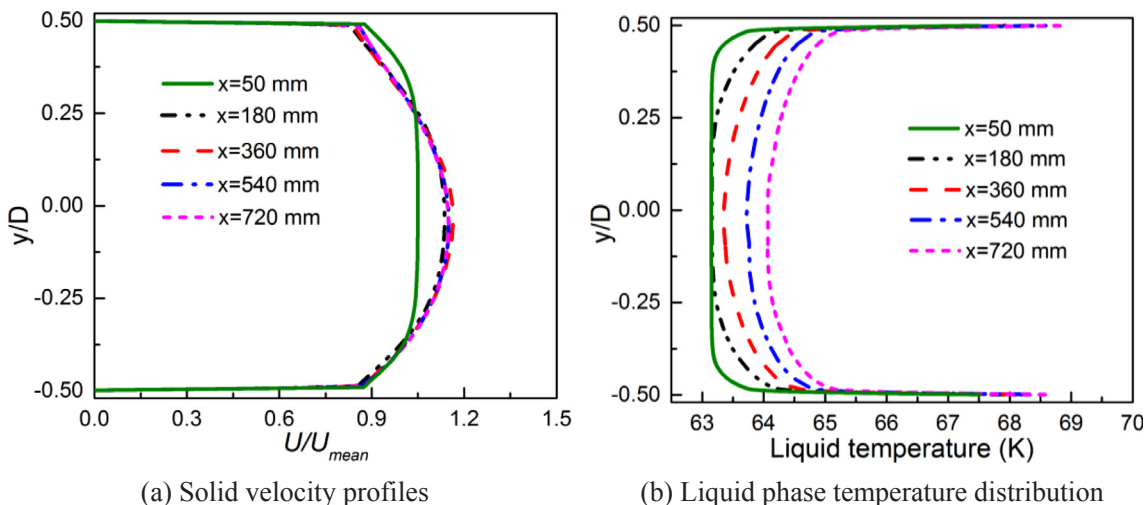
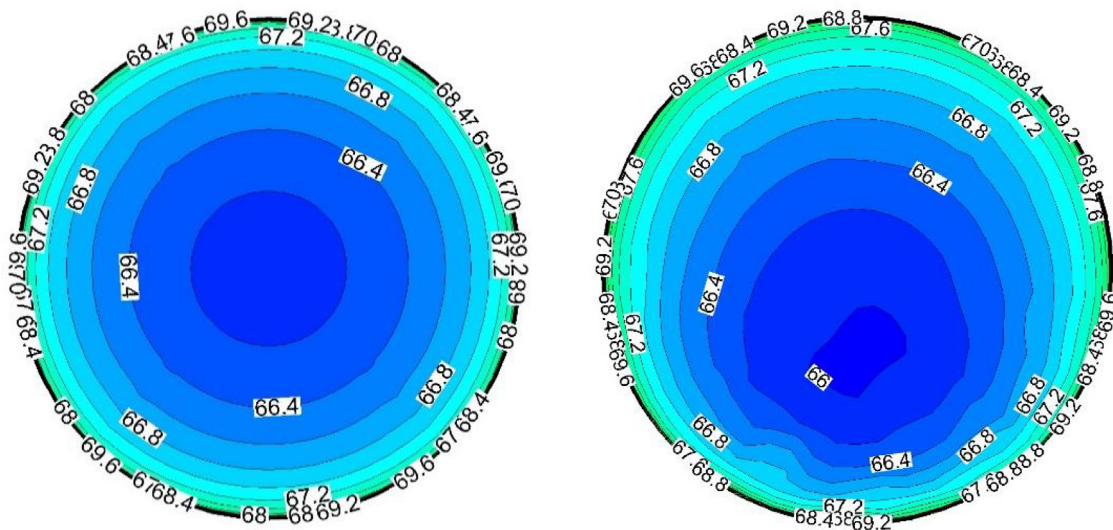


Fig. 6. Results for solid velocity and liquid phase temperature of slush nitrogen ($\alpha_s = 10\%$, $U_{in} = 1$ m/s) along the test pipe.



(a) Subcooled liquid nitrogen

(b) Slush nitrogen ($\alpha_s=10\%$)

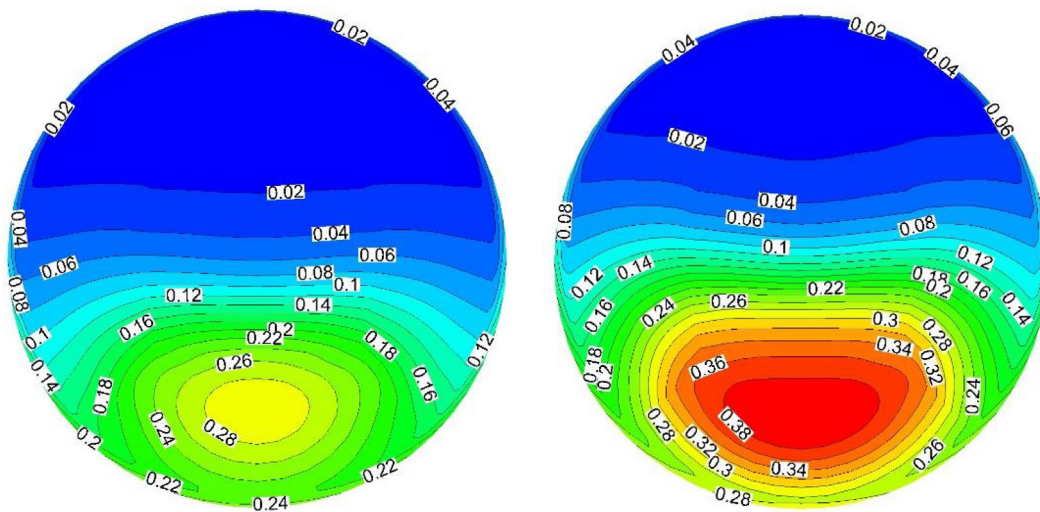
Fig. 8. Contours of temperature profiles (K) of liquid phase at $x = 720$ mm.

decreases with an increasing solid fraction due to the concentration of solid particles in the bulk region. As for the wall temperature, it can be seen that the upper wall temperature decreases with increasing solid fraction, while the lower wall temperature increases with increasing solid fraction. Actually, the heat transfer between the pipe wall and fluid is within the near-wall thermal boundary layer, which is mainly composed of liquid nitrogen. The heat transfer of the liquid phase can be suppressed or enhanced due to the particles motion, and whether the heat transfer is suppressed or enhanced depends on the particle concentration. Thus, the heat transfer of the liquid nitrogen near the lower wall is suppressed by the high concentration of particles while the heat transfer near the upper wall is promoted by the very dilute particles. On the other hand, the average temperature of the bulk zone of slush nitrogen with higher particle concentration is lower than that of the dilute slush nitrogen.

In the present study, under the condition of constant heat flux, when the heat transfer temperature difference of slush nitrogen is higher than

that of liquid nitrogen, the heat transfer coefficient can be relatively low. For the slush nitrogen with higher solid fraction, the forced convection heat transfer of the liquid phase is suppressed by the high concentration particle distribution, which results in poorer heat transfer performance for the slush nitrogen with higher particle concentration.

The turbulent motion of particles can also have a significant effect on the forced convection heat transfer of the liquid phase of slush nitrogen. Fig. 11 gives the contours for turbulent kinetic energy of the liquid phase of slush nitrogen and the subcooled liquid nitrogen with an inlet flow velocity of 0.5 m/s at the plane of $Z = 0$. Fig. 12 also gives the distribution of turbulent kinetic energy of the liquid phase for subcooled liquid nitrogen and slush nitrogen in the fully developed region. Compared with the contours of particle concentration in Fig. 9(a), it can be concluded that the turbulent kinetic energy of the near-wall liquid phase of slush nitrogen, especially where the particles concentrate, is relatively low. It can be seen that high concentrated particles could inhibit the turbulent energy of the near-wall liquid phase, which



(a) $\alpha_s=10\%$

(b) $\alpha_s=20\%$

Fig. 9. Contours of particle concentration profiles of slush nitrogen at $x = 720$ mm.

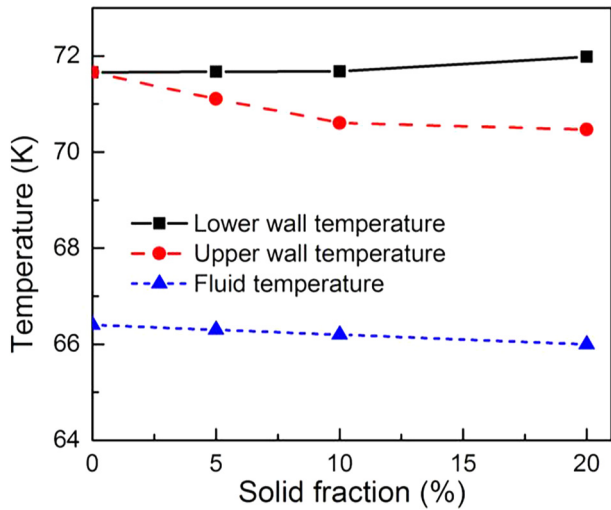


Fig. 10. Variation of wall and fluid temperature of liquid phase with solid fraction of slush nitrogen.

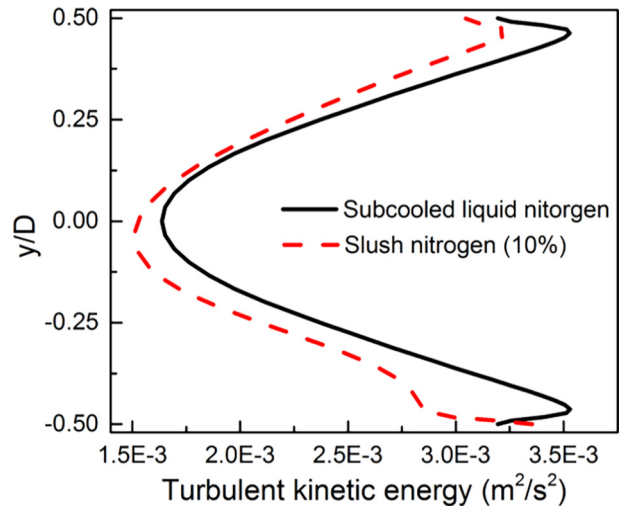
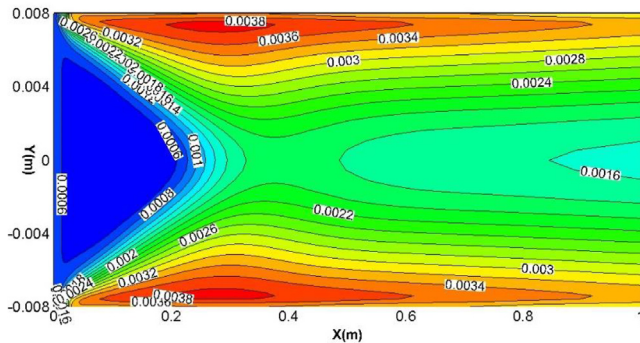
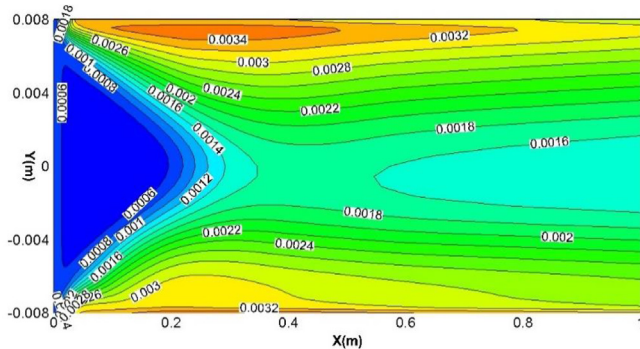


Fig.12. Profiles of the turbulent kinetic energy of liquid phase (at the velocity of 0.5 m/s).



(a) Subcooled liquid nitrogen (m^2/s^2)



(b) Slush nitrogen ($\alpha_s=0.1$) (m^2/s^2)

Fig.11. Contours of turbulent kinetic energy of liquid phase (at the velocity of 0.5 m/s).

suppresses the mixing of the hot and cold fluids and results in deteriorated near-wall forced convection heat transfer. Compared with the subcooled liquid nitrogen, the forced convection of the liquid phase is weakened and the heat conduction towards the central area is reduced. This leads to the deterioration of the heat transfer performance of slush nitrogen.

According to Eq. (13), the particle diameter is a key factor for interfacial heat transfer. The interphase heat transfer coefficient of particle-fluid should decrease with increasing particle size. In addition, the pipe diameter is also an important factor for the heat transfer

deterioration of slurry flows [10]. To discuss the influence of pipe diameter D and particle size d_s on the heat transfer performance of slush nitrogen, the slush nitrogen flows with the different initial size ratios between pipe and particle are investigated. Fig. 13 presents the numerical results for local heat transfer coefficient of slush nitrogen with different diameter ratio D/d_s and flow velocity comparing to subcooled liquid nitrogen, where $r = D/d_s$. The results are for the slush nitrogen with a solid fraction of 10% and a flow velocity of 0.5–4 m/s. At low velocity, the heat transfer coefficient of slush nitrogen is higher than that of the subcooled liquid nitrogen for different D/d_s . And as flow velocity increases, the heat transfer of slush nitrogen deteriorates compared to the subcooled liquid nitrogen. The heat transfer coefficient ratio of slush nitrogen and subcooled liquid nitrogen is illustrated in Fig. 14. For the pipe diameter of 10 mm, the critical velocity for the deterioration is around 3 m/s, while it is around 1 m/s for the pipe diameter of 16 mm, which means that the heat transfer deterioration of slush nitrogen tends to occur for slush nitrogen flow in the larger pipe at a higher flow velocity.

Fig. 15 gives the results for local heat transfer coefficients, wall temperature and fluid temperature with the particle diameters of 1 mm and 2 mm for the pipe with a diameter of 16 mm, where h_{local} is the local heat transfer coefficient at $x = 720$ mm, T_w is the wall temperature and T_f is the bulk fluid temperature. As in Fig. 15, the temperature difference between the wall and bulk fluid of the cases for 2 mm particles is lower than that for 1 mm particles, so the heat transfer coefficient of slush nitrogen with 2 mm particles is lower than that of slush nitrogen with 1 mm particles.

Fig. 16 illustrates the results for turbulent kinetic energy along the vertical direction at $x = 720$ mm of slush nitrogen ($\alpha_s = 10\%$) with different pipe and particle diameter. The pipe and particle size both have obvious influence on the turbulence and heat transfer of liquid phase. At flow velocity of 2 m/s, the turbulent kinetic energy of the liquid phase of the smaller pipe is greater than that for the larger pipe, especially in the near-wall region, which results in a better heat transfer performance in smaller pipes. In addition, as presented in Fig. 16(b), the concentration of particles with larger size helps to suppress the turbulent kinetic energy of the liquid phase, especially for the lower region where the particles gather. Thus, the mixing of the hot and cold fluids is inhibited, which results in weaker forced convection of the liquid phase.

3.4. Heat transfer correlation of slush nitrogen

The flow regimes need to be considered when assessing heat

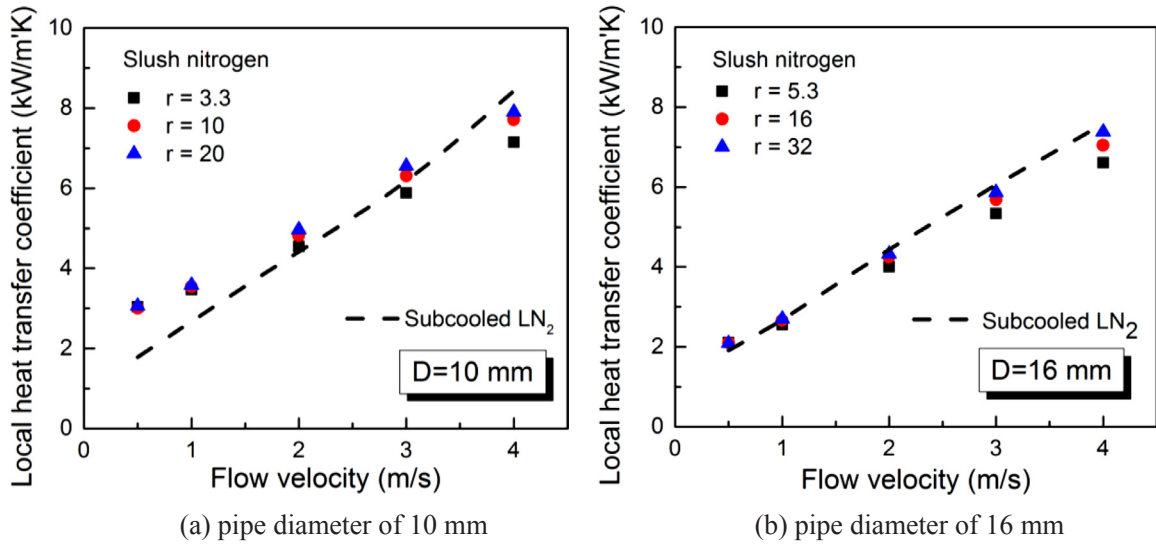


Fig. 13. Local heat transfer coefficient of slush nitrogen ($\alpha_s = 10\%$) with different r and velocity.

transfer correlations for turbulent slurry flow inside a tube. The heat transfer correlation for homogeneous and heterogeneous flows involving slush properties is given by Orr-Dallavalle equation as [22]

$$Nu_{sl} = 0.027Re_{sl}^{0.8}Pr_{sl}^{1/3} \left(\frac{\mu_l}{\mu_{lv}} \right)^{0.14} \quad (30)$$

where the Prandtl number of slurry is defined by $Pr_{sl} = \mu_m c_{p,sl} / \lambda_{sl}$ and $c_{p,sl}$ is the heat capacity of slurry and λ_{sl} is the slush thermal conductivity.

For sliding bed flow and compaction flow, the two-phase Nusselt number is given by Reeves [23] as

$$Nu_{sl} = Nu_l \left(1 + 0.00224\alpha_s Fr \left/ \left(\frac{\rho_s}{\rho_l} - 1 \right) \right. \right) \quad (31)$$

where Nu_l is the single phase Nusselt number, obtained by

$$Nu_l = 0.0384Re_l^{3/4}Pr_l \left/ \left(1 + \frac{1.50(P\eta - 1)}{Re_l^{1/8}Pr_l^{1/6}} \right) \right. \quad (32)$$

Fr is the Froude number, $Fr = U_{ave}^2 / (gD)$, where U_{ave} is the average fluid velocity and D is the pipe diameter.

Based on the slush nitrogen experimental data, Jiang and Zhang [6] obtained the experimental empirical correlations for Nusselt number as

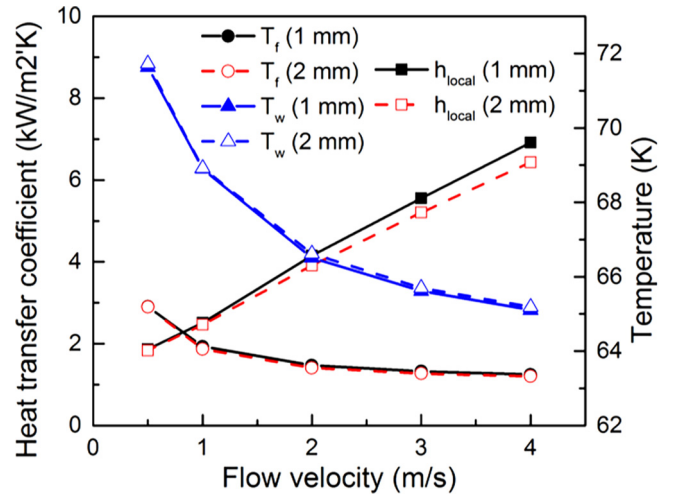


Fig. 15. Heat transfer coefficient and temperature for slush nitrogen ($\alpha_s = 10\%$) with different particle diameter at $x = 720$ mm.

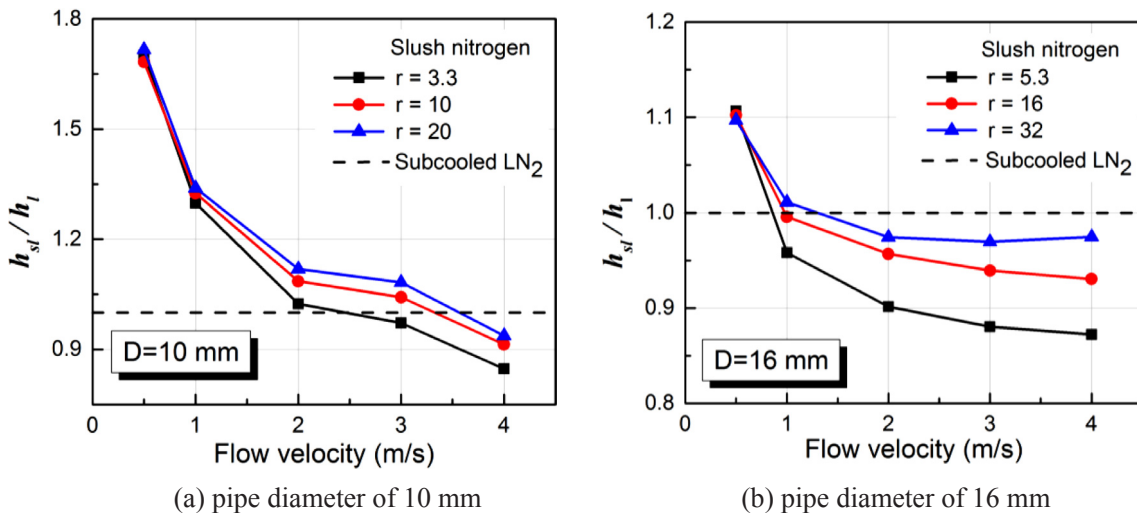


Fig. 14. Heat transfer coefficient ratio h_{sl}/h_l of slush nitrogen ($\alpha_s = 10\%$) with different r and velocity.

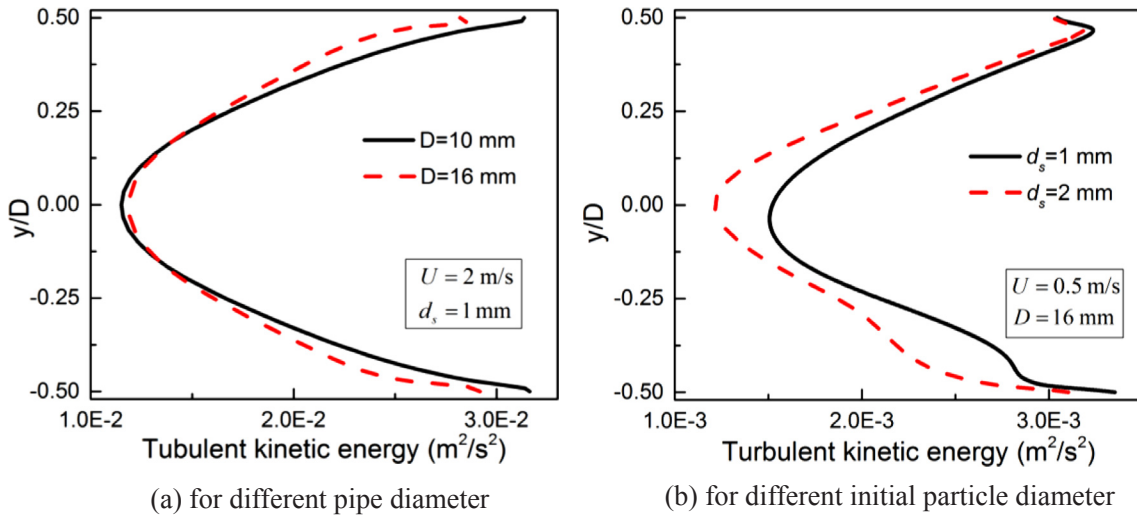


Fig. 16. Turbulent kinetic energy of liquid phase for slush nitrogen ($\alpha_s = 10\%$) with different pipe and particle diameter along vertical direction at $x = 720$ mm

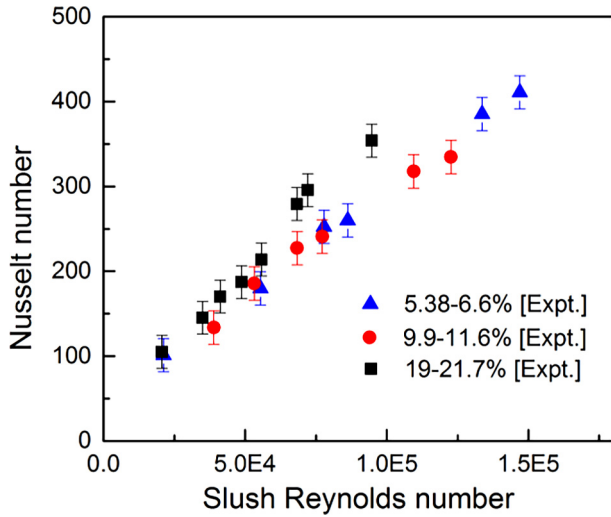


Fig. 17. Relation of Nusselt number with slush Reynolds number.

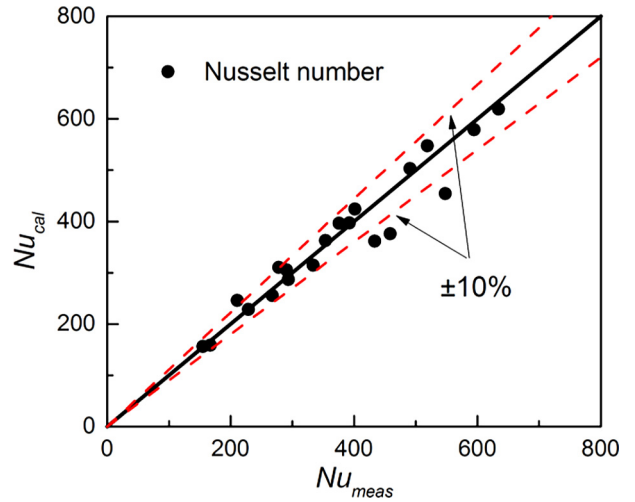


Fig. 19. Comparison of empirical correlation results with experimental results

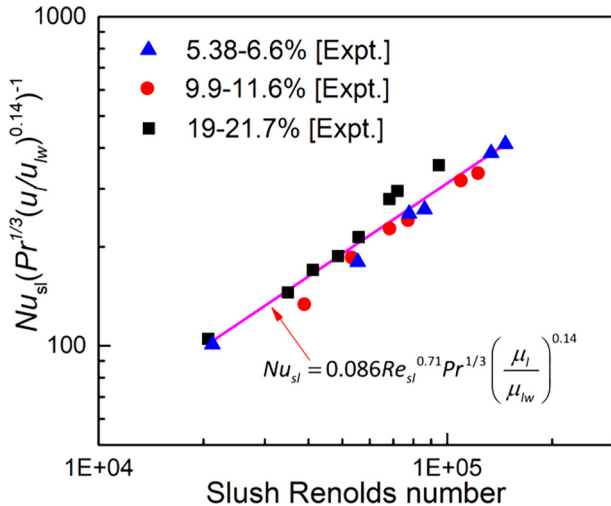


Fig. 18. Fitting of modified Nusselt number with slush Reynolds number.

$$Nu_{sl} = 0.0792 Ste^{-0.05} \left(\frac{\alpha_s}{\alpha_l} \right)^{0.5} Re_{sl}^{0.8} Pr^{1/3} \left(\frac{\mu_l}{\mu_{lw}} \right)^{0.14} \quad (2.42)$$

$$\times 10^4 < Re_{sl} < 6.23 \times 10^4 \quad (33)$$

where Ste is the Stefan number, given by $Ste = c_p \Delta T_{sl} / h_{melt}$, c_p is the specific heat of liquid phase for melting process, ΔT_{sl} is the temperature difference between phases. The adoption of Stefan number was claimed to be helpful for the consideration of the melting process. However, for the case of slush nitrogen pipe flow, ΔT_{sl} is rather small (no more than 1 K) and c_p and h_{melt} are almost constant, which makes the Stefan number to remain almost constant. It is difficult to state that the Stefan number can play an actual role when considering the interfacial mass transfer of slush nitrogen.

According to our earlier experimental work on slush nitrogen flow field [24], the flow regime of slush nitrogen evolves into sliding bed flow, heterogeneous flow and homogenous flow as the slush Reynolds number increases. However, to calculate the Nusselt number for slush nitrogen by Eqs. (30–32), the flow regime needs to be predicted firstly by the flow regime map [23], which results in complexity of the solution. The present experimental data at different flow regimes are analyzed in order to obtain an improved experimental empirical heat transfer correlation for slush nitrogen flow. As given in Fig. 17, the slush Reynolds number is adopted to correlate the Nusselt number. The modified Nusselt number is calculated by $Nu_{sl} [Pr_{sl}^{1/3} (\mu_l / \mu_{lw})^{0.14}]^{-1}$.

Fig. 18 illustrates the heat transfer correlation for Nusselt number and slush Reynolds number as follows

$$Nu_{sl} = 0.086 Re_{sl}^{0.71} Pr_{sl}^{1/3} \left(\frac{\mu_l}{\mu_{lw}} \right)^{0.14} \quad (1.1 \times 10^4 < Re_{sl} < 1.1 \times 10^5) \quad (34)$$

The slush Reynolds number is based on the Cheng and Law equation, as given by

$$Re_{sl} = \rho_{sl} v D / \mu_m \quad (35)$$

where μ_m is the slush effective viscosity. The Cheng and Law equation, i.e., Eq. (12), is adopted to calculate the slush effective viscosity and the slush Reynolds number of slush nitrogen. It should be noted that, the slush Reynolds number in the Orr-Dallavalle equation is calculated by $\mu_{sl} = \mu_l [1 - (\alpha_s / \alpha_{s,max})]^{-1.6}$. The maximum particle concentration $\alpha_{s,max}$ depends on the size and shape of particles, which results in a complex determination. For the Cheng and Law equation, it is not necessary to involve the maximum particle concentration in computing the effective viscosity, the parameters are determined by the particle size, shape and type. Moreover, the Cheng and Law equation has higher accuracy, especially for high concentration slurries [24].

Thus, the empirical correlation given by Eq. (34) has taken the particle conditions into consideration, and can better characterize the heat transfer performance of slush nitrogen at different flow regimes. Comparison of the calculated results from this correlation with the experimental results is presented in Fig. 19, indicating the improved accuracies within a band of $\pm 10\%$.

4. Conclusions

Slush nitrogen can be a potential alternative coolant for high temperature superconducting cables with lower temperature, higher heat capacity and density than subcooled liquid nitrogen. The heat transfer performance of slush nitrogen flow in a horizontal pipe with a diameter of 16 mm was experimentally and numerically investigated. An experimental apparatus for the heat transfer test of slush nitrogen flow was set up and the heat transfer coefficients of slush nitrogen and subcooled liquid nitrogen flows in a horizontal pipe were measured under the operating conditions of the flow velocity of 0–4 m/s, the solid fraction of 0–23%, and the wall heat flux of 12–15 kW/m².

The numerical and experimental results show good agreement on the temperature distribution and heat transfer coefficients. The local heat transfer coefficient of slush nitrogen is lower than that of subcooled liquid nitrogen at the same flow velocity, and decreases with the increasing solid fraction. The mechanisms for heat transfer deterioration of slush nitrogen were discussed by analyzing the effect of the particle concentration and size, the pipe size and the flow velocity on the forced convection of slush nitrogen and the solid-liquid interfacial heat transfer.

The results for the turbulent kinetic energy of the liquid phase show that the dominating reason for the heat transfer deterioration of slush nitrogen is that the gathering of particles suppresses the force convection of the liquid phase of slush nitrogen. As the solid particles accumulate, the turbulent kinetic energy of liquid phase is inhibited, so that the mixing of the hot and cold fluids of slush nitrogen deteriorates. In fact, the whole heat conduction from the wall toward the central area is suppressed, which leads to the deterioration of the heat transfer performance of slush nitrogen compared to that of subcooled liquid nitrogen. On the other hand, the concentration of particles with larger size also causes the decrease of the turbulent kinetic energy of liquid phase, which results in weaker solid-liquid interfacial heat transfer and heat convection of liquid phase.

An experimental empirical correlation for Nusselt number of slush nitrogen with the slush Reynolds number was obtained, with a deviation within $\pm 10\%$ from the experimental results. The improvement

provided by this empirical correlation resides in that it is applicable for different flow regimes (i.e., homogenous flow, heterogeneous flow and sliding bed flow). Moreover, the correlation with the slush Reynolds number takes the influences of the particle size, type and shape on the interfacial heat and mass transfer into consideration.

5. Conflict of interest

None.

Acknowledgment

This work was financially supported by the National Key Basic Research Program of China (No. 613322). Yijian Li is grateful for the support of the China Scholarship Council, China.

References

- [1] J.G. Bednorz, K.A. Müller, Possible high Tc superconductivity in the Ba-La-Cu-O system, *Z. Phys. B Condens. Matter* 64 (2) (1986) 189–193.
- [2] E. Shabagin, C. Heidt, S. Strauß, S. Grohmann, Modelling of 3D temperature profiles and pressure drop in concentric three-phase HTS power cables, *Cryogenics* 81 (2017) 24–32.
- [3] J. Ishimoto, R. Ohno, H. Yanagi, A. Machida, M. Ikeuchi, K. Hattori, et al., Basic study on two-phase flow characteristics of slush nitrogen in a pipe, *Advances in Cryogenic Engineering: Transactions of the Cryogenic Engineering Conference, AIP Publishing*, 2004, pp. 1099–1106.
- [4] K. Ohira, Study of nucleate boiling heat transfer to slush hydrogen and slush nitrogen, *Heat Transfer-Asian Res.* 32 (1) (2003) 13–28.
- [5] K. Matsuo, M. Ikeuchi, A. Machida, K. Yasuda, Fundamental study of pipe flow and heat transfer characteristics of slush nitrogen, *Advances in Cryogenic Engineering: Transactions of the Cryogenic Engineering Conference, AIP Publishing*, 2006, pp. 1033–1040.
- [6] P. Zhang, Y.Y. Jiang, Forced convective heat transfer of slush nitrogen in a horizontal pipe, *Int. J. Heat Mass Transfer* 71 (1) (2014) 158–171.
- [7] K. Ohira, K. Nakagomi, N. Takahashi, Pressure-drop reduction and heat-transfer deterioration of slush nitrogen in horizontal pipe flow, *Cryogenics* 51 (10) (2011) 563–574.
- [8] K. Ohira, J. Okuyama, K. Takahashi, I. Aoki, Pressure drop reduction and heat transfer deterioration of slush nitrogen in triangle pipe flow. *International Congress of Refrigeration*. Yokohama, Japan, 2015.
- [9] B. Knodel, D. France, U. Choi, M. Wambsgans, Heat transfer and pressure drop in ice-water slurries, *Appl. Therm. Eng.* 20 (7) (2000) 671–685.
- [10] K.V. Liu, U.S. Choi, K.E. Kasza, Measurements of pressure drop and heat transfer in turbulent pipe flows of particulate slurries. Argonne National Laboratory Report, ANL-88-15, 1988.
- [11] J. Ishimoto, R. Ono, Numerical study of the two-phase flow characteristics of slush nitrogen, *Cryogenics* 45 (4) (2005) 304–316.
- [12] K. Ohira, A. Ota, Y. Mukai, T. Hosono, Numerical study of flow and heat-transfer characteristics of cryogenic slush fluid in a horizontal circular pipe (SLUSH-3D), *Cryogenics* 52 (7) (2012) 428–440.
- [13] T. Jin, Y. Li, S. Wu, Y. Liu, Numerical modeling for the flow and heat transfer of slush nitrogen in a horizontal pipe based on population balance equations, *Appl. Therm. Eng.* 123301–9 (2017).
- [14] T. Jin, Y.J. Li, Z.B. Liang, Y.Q. Lan, G. Lei, X. Gao, Numerical prediction of flow characteristics of slush hydrogen in a horizontal pipe, *Int. J. Hydrogen Energy* 42 (6) (2017) 3778–3789.
- [15] Y. Li, S. Wu, T. Jin, G. Lei, Experimental study on the performance of capacitance-type meters for slush nitrogen measurement, *Exp. Therm. Fluid Sci.* 88 (2017) 103–110.
- [16] N.S. Cheng, A.W.K. Law, Exponential formula for computing effective viscosity, *Powder Technol.* 129 (1–3) (2003) 156–160.
- [17] S. Kumar, D. Ramkrishna, On the solution of population balance equations by discretization - III. Nucleation, growth and aggregation of particles, *Chem. Eng. Sci.* 52 (24) (1997) 4659–4679.
- [18] D.L. Marchisio, R.D. Vigil, R.O. Fox, Quadrature method of moments for aggregation–breakage processes, *J. Colloid Interface Sci.* 258 (2) (2003) 322–334.
- [19] D.L. Marchisio, R.D. Vigil, R.O. Fox, Implementation of the quadrature method of moments in CFD codes for aggregation–breakage problems, *Chem. Eng. Sci.* 58 (15) (2003) 3337–3351.
- [20] L. Schiller, A. Naumann, A drag coefficient correlation, *Z. Ver. Deutsch. Ing.* 77 (1935) 318–320.
- [21] N. Sieder, G.E. Tate, Heat transfer and pressure drop of liquids in tubes, *Ind. Eng. Chem.* 28 (12) (1936) 1429–1435.
- [22] C. Orr, J.M. DallaValle, Heat transfer properties of liquid-solid suspensions, *Chem. Eng. Prog.* 50 (9) (1954) 29–45.
- [23] S.A. Reeves, Heat transfer in two-phase (solid-liquid) single-component flow. Master thesis, Ruston, LA: Louisiana Tech University, 1968.
- [24] T. Jin, Y. Li, S. Wu, J. Wei, Flow field and friction factor of slush nitrogen in a horizontal circular pipe, *Cryogenics* 91 (2018) 81–95.